IEEE Access
Multidisciplinary ⋮ Rapid Review ⋮ Open Access Journal

Received September 13, 2019, accepted September 23, 2019, date of publication January 2, 2020, date of current version January 8, 2020.

*Digital Object Identifier 10.1109/ACCESS.2019.2950284*

# Mechanism and Method for Outer Raceway Defect Localization of Ball Bearings

**FEIBIN ZHANG[1], JINFENG HUANG[2], (Student Member, IEEE), FULEI CHU[1], AND LINGLI CUI[2], (Member, IEEE)**

[1]Department of Mechanical Engineering, Tsinghua University, Beijing 100084, China
[2]Beijing Engineering Research Center of Precision Measurement Technology and Instruments, Beijing University of Technology, Beijing 100124, China

Corresponding author: Fulei Chu (chufl@mail.tsinghua.edu.cn)

This work was supported by the National Key Research and Development Program of China under Grant 2018YFB1306100.

**ABSTRACT** The localization of outer raceway defect plays a significant role in malfunction elimination, failure cause analysis as well as the residual life prediction of ball bearings. Based on the nonlinear dynamic model for a ball bearing and the outer raceway defect model considering the ball finite size, this article employs the detailed mathematical derivation and theoretical analysis of the load distribution for the bearing system with an outer raceway defect located at the different angular positions. Therefore, the essential mechanism of the approximate linear relationship between the proposed indices, namely horizontal–vertical synchronized Peak (HVSPeak) and horizontal–vertical synchronized RMS (HVSRMS), and the defect angular position is explained. More importantly, it is theoretically demonstrated that HVSRMS is approximately a cotangent function with the defect angular position as the only variable, which indicates that the index has excellent anti-interference and practicability. In addition, the superiority and necessity of the HVSRMS index can be seen when compared to HVSPeak, RMS, SampEn and Lemple-Ziv. It is validated through simulation and experiment results that HVSRMS index can efficiently diagnose the angular position of outer raceway defect. Finally, the signal denoising methods for HVSRMS are compared and studied, which indicates the direction for subsequent research.

**INDEX TERMS** Defect localization, HVSRMS, ball bearing, fault diagnosis.

## I. INTRODUCTION

The mechanism and method of fault diagnosis for ball bearings is a continuous research focus. With the development of theory and technology, the research hotspot from qualitative diagnosis to quantitative diagnosis is gradually becoming a trend. The quantitative diagnosis for an outer raceway defect mainly includes two aspects: defect size estimation and defect angular position estimation. The angular position estimation of the outer raceway defect, namely the localization diagnosis of outer raceway defect mainly has the following important significance or application value [1]: 1) The defect angular position is one of the main factors affecting the residual life prediction of the bearing; for example, in the case of all other factors held constant, the defect closer to the load center may have a faster expansion speed making the residual life of the bearing also shorter. 2) Different angular positions of outer raceway defects may correspond to different failure causes; for example, if a defect happens close to the load center, it mainly caused by fatigue damage; but if the defect occurs far away from the load center, the cause is more likely to be the machining defects, maintenance defect, or others.

In recent years, scholars have carried out a large number of systematic studies on the quantitative diagnosis mechanism and method of the defect size of rolling bearing and have obtained some remarkable achievements that enhanced the scholarship. If a rolling element bearing has a local fault, a series of impulses with certain laws will be generated in its time-domain waveform [2], [3], so vibration signals are used widely for the fault diagnosis of bearing [4]–[9]. However, bearing fault signatures are usually contaminated or even overwhelmed by interfering noise [10]. In such circumstances, a method for noise reduction and feature extraction is needed, such as wavelet transform, sparse representation and empirical mode decomposition [11]–[14]. A technique based on decomposition Symlet wavelet was employed for

The associate editor coordinating the review of this manuscript and approving it for publication was Dazhong Ma.

estimating the inner raceway defect width [15]. To separate the entry-exit events, and to calculate the size of the fault, the approximate entropy method and empirical mode decomposition were applied by Ref. [16]. Zhao *et al.* [17] presented a methodology for the detection and recovery of fault impulses, with which the double impact phenomenon caused by a distributed defect was extracted successfully, so the defect size of a bearing can be estimated from its vibration signal without dismantling the component. An averaged dual-impulse interval determining method was used to evaluate the spall size [18]. For the fault diagnosis, the mechanism of fault is indispensable, which gives reasons and characteristics of fault changes. Many models of ball bearing have been established by scholars to research and reveal the defect generation mechanism and characteristic. A dynamic model with six DOFs was developed to investigate vibrations of high-speed rolling ball bearings with localized surface defects on raceways [19]. Khanam et al. [20] proposed an analytical force modeling approach based on the principles of engineering mechanics to explain the mechanism of excitation generation due to the impact of ball mass against the defect edge. Cui *et al.* [21] established a nonlinear dynamic model of rolling element bearings for assessment of the severity of an outer race fault, and analyzed quantitatively the correlation between vibration responses and fault sizes based on the model. Liu *et al.* [22] proposed a local fault model which includes the time-varying displacement impulse and contact stiffness, and the relationship between the contact stiffness and fault sizes was obtained through this method. Petersen *et al.* [23] pointed out that faults which differ in size by natural multiples of the rolling element angular spacing have the same vibration time interval based on the established dynamic model, and then proposed a valid method to distinguish those faults.

The above research are carried out around the mechanism and method of outer raceway defect size estimation. However, the research aiming at the localization diagnosis of outer raceway defect is almost unreported. The main reasons linked to two factors, the first is sparse breakthroughs in the mechanism research. The second is the lack of the single factor characteristics of the localization diagnosis, which is not affected by the noise and the inherent characteristics of the system such as the defect characteristic frequency in the qualitative diagnosis and the time interval between double impact points in quantitative diagnosis. Cui *et al.* [1], [24] preliminarily explored the localization diagnosis of the outer raceway defect based on the proposed horizontal–vertical synchronized RMS (HVSRMS) index. However, the inherent mechanism of the index has not been excavated. Therefore, based on the nonlinear dynamic model for a ball bearing and the outer raceway defect model considering ball finite size, the detailed mathematical derivation and theoretical analysis of dynamic behavior for ball bearings with an outer raceway defect located at different angular position are researched in this paper. Hence, the essential mechanism of the approximate linear relationship between HVSRMS and the defect angular position is explained. Furthermore, the superiority and necessity of HVSRMS index is validated through the comparison to other indices, including horizontal-vertical synchronized Peak (HVSPeak), RMS, SampEn and Lemple-Ziv.

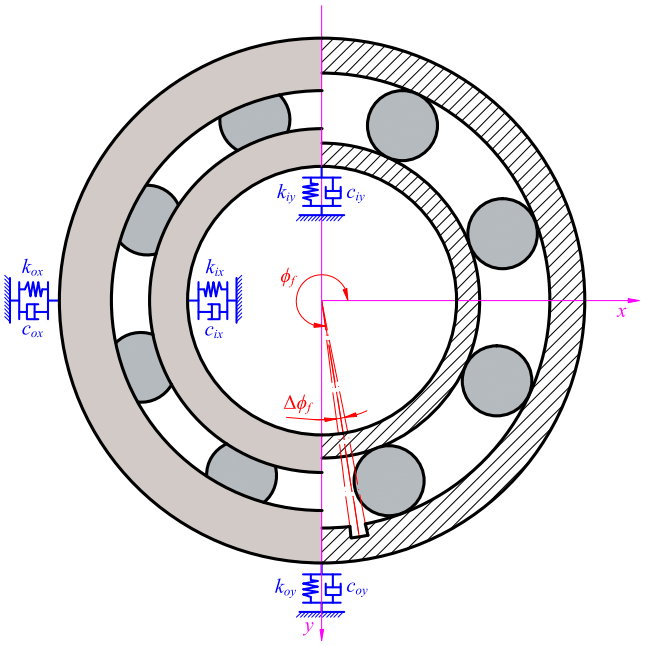


**FIGURE 1.** Nonlinear dynamic model of a ball bearing system.

This paper is organized as follows. Section II establishes the static model of a ball bearing with an outer raceway defect and introduces the theory of horizontal–vertical synchronization eigenvalue. In Section III, the dynamic model of a ball bearing with an outer raceway defect is established and the horizontal – vertical synchronization signal analysis is implemented, where the mechanism of the approximate linear relationship between HVSRMS and the defect angular position is explained. In Section IV, the experiment is carried out to evaluate the performance of the proposed method. A comparison between the proposed index and other indices, such as RMS, SampEn and Lemple-Ziv is also presented. Concluding remarks are presented in Section V.

## II. STATIC MODEL AND THE THEORY OF HORIZONTAL -VERTICAL SYNCHRONIZATION INDEX

### A. STATIC MODEL AND FAULT-FREE SYSTEM ANALYSIS

Figs. 1 and 2 represent the diagrams of a dynamic model of the ball bearing and outer raceway defect model, respectively. $m_i$ and $m_o$ are the masses of the inner race and outer race. $(c_{ix}, c_{iy})$, $(k_{ix}, k_{iy})$ and $(x_i, y_i)$ are the damping, stiffness and displacement of the inner race, $(c_{ox}, c_{oy})$, $(k_{ox}, k_{oy})$ and $(x_o, y_o)$ are the damping, stiffness and displacement of the outer race. $W_x$ and $W_y$ are the loads in the $x$ and $y$ directions. The static equilibrium equations of inner race can be expressed as:

$$\begin{bmatrix} W_x \\ W_y \end{bmatrix} = \begin{bmatrix} \bar{Q}_x \\ \bar{Q}_y \end{bmatrix} = \sum_{j=1}^{N_b} \begin{bmatrix} \bar{Q}_{j,x} \\ \bar{Q}_{j,y} \end{bmatrix} = \sum_{j=1}^{N_b} \begin{bmatrix} K\left(\delta_j\right)_+^{1.5} \cos\phi_j \\ K\left(\delta_j\right)_+^{1.5} \sin\phi_j \end{bmatrix} \quad (1)$$

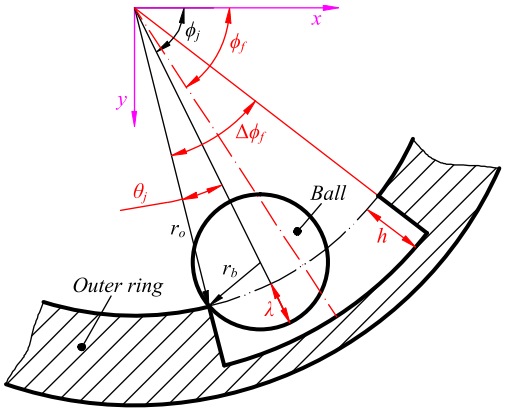


**FIGURE 2.** Diagram of a ball over the defect.

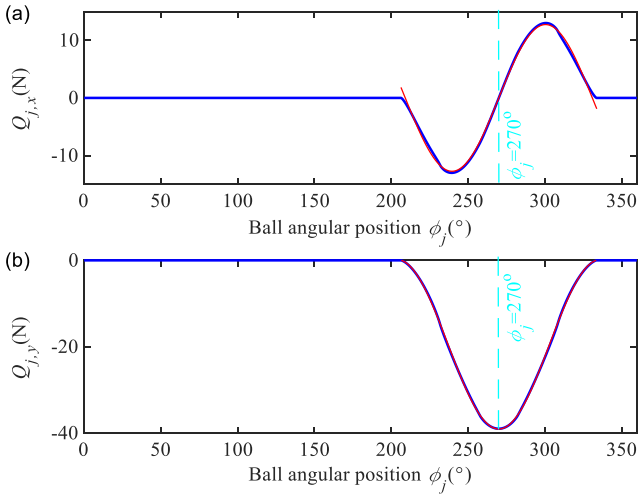


**FIGURE 3.** Static contact forces of the ball $j$ for a failure-free bearing system: (a) Horizontal component of contact force $\bar{Q}_{j,x}(\phi_j)$; (b) Vertical component of contact force $\bar{Q}_{j,y}(\phi_j)$.

where $N_b$ is the number of balls, $\bar{Q}_{j,x}$ and $\bar{Q}_{j,y}$ are the static contact forces between ball $j$ and raceway in the $x$ and $y$ directions, respectively. $(\,)_+$ represents negative setting zero. The angular position $\phi_j$ of the ball $j$ can be given by:

$$\phi_j = \phi_1 + \frac{360^o}{N_b}(j-1) \tag{2}$$

$\delta_j$ is the contact deformation of the ball $j$. It can be defined as:

$$\delta_j = \delta_x \cos\phi_j + \delta_y \sin\phi_j - r_l - d(\phi_j) \tag{3}$$

where $\delta_x = x_o\text{-}x_i$ and $\delta_y = y_o\text{-}y_i$ are the relative displacements between the inner and outer race in the $x$ and $y$ directions, $r_l$ is the radial clearance, $d(\phi_j)$ is the effective defect depth. For the defect model shown in Fig. 2, $d(\phi_j)$ is defined as:

$$d(\phi_j) = r_o\left(\cos\left(\theta_j\right) - 1\right) + r_b - \sqrt{r_b^2 - r_o^2\sin^2\left(\theta_j\right)} \tag{4}$$

$\bar{Q}_{j,x}(\phi_j)$ and $\bar{Q}_{j,y}(\phi_j)$ loaded on the ball $j$ in random angular position $\phi_j$ can be calculated by Eqs. (1)-(4). Taking

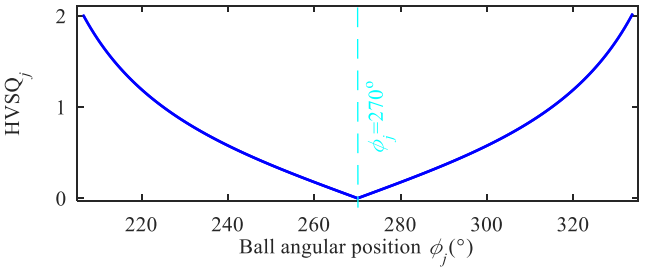


**FIGURE 4.** Horizontal-vertical synchronization contact force $\text{HVS}\bar{Q}_j(\phi_j)$.

NSK6308 bearing as an example, set $W_x = 0$, $W_y = -100$, The other parameter values of the bearing system can be found in [1]. Fig. 3 shows the variation curve of $\bar{Q}_{j,x}(\phi_j)$ and $\bar{Q}_{j,y}(\phi_j)$ in a complete rotation period in the failure-free case which illustrates that the load interval is [206.3°, 333.8°] in this case. Furthermore, the curves of $\bar{Q}_{j,x}$ and $\bar{Q}_{j,y}$ varying with $\phi_j$ are approximate the sine and versine curves centered at 270°, respectively, and both have the same frequency $f_q$ and phase $\varphi_q$. The sine and versine function curves obtained by the data fitting using the lsqcurvefit function of MATLAB are shown as a red line in Fig. 3, and its expressions can be described as follows

$$\begin{cases} \bar{Q}_{j,x} = -A_x \sin\left(2\pi f_q \phi_j + \varphi_q\right) \\ \bar{Q}_{j,y} = -A_y \,\text{versin}\left(2\pi f_q \phi_j + \varphi_q\right) \end{cases} \tag{5}$$

where $A_x, A_y, B_y, f_q, \varphi_q$ are the coefficients of the fitting function. It is revealed by combining with Fig. 3 and Eq. (5) that in the load interval and regarding $\phi_j = 270°$ as a starting point, there is no monotonic mapping relationship between $\bar{Q}_{j,x}$ and $\phi_j$, and the inflection points are 239.4° and 300.7°, while there is a monotonic mapping relationship between $\bar{Q}_{j,y}$ and $\phi_j$, but the curve around 270° changes slightly. To excavate the characteristic indices with a simple and effective mapping relationship with $\phi_j$, horizontal-vertical synchronization contact force $\text{HVS}\bar{Q}_j$ is proposed as follows

$$\begin{aligned} \text{HVS}\bar{Q}_j &= \left|\frac{\bar{Q}_{j,x}}{\bar{Q}_{j,y}}\right| = \left|\frac{K\left(\delta_j\right)_+^{1.5}\cos\phi_j}{K\left(\delta_j\right)_+^{1.5}\sin\phi_j}\right| = \left|\cot\phi_j\right| \\ &= \left|\frac{-A_x\sin\left(2\pi f_q\phi_j + \varphi_q\right)}{A_y\,\text{versin}\left(2\pi f_q\phi_j + \varphi_q\right)}\right| \\ &= \frac{A_x}{A_y}\left|\cot(\pi f_q\phi_j + \frac{\varphi_q}{2})\right| \end{aligned} \tag{6}$$

Fig. 4 presents the results of $\text{HVS}\bar{Q}_j$ in the load interval. The comparison between Fig. 3 and Fig. 4 shows that the relationship between $\text{HVS}\bar{Q}_j$ and $\phi_j$ is the simplest, especially in the range of $\phi_j = 240° \sim 300°$, $\text{HVS}\bar{Q}_j$ values are approximately two straight lines with symmetrical about $\phi_j = 270°$. Since the contact force between the ball and raceway is the main excitation source of faulty bearing, it can be expected that this feature will provide a very effective support for excavating localization diagnosis characteristics for outer raceway defect.

To verify the applicability scope of this characteristic, the mapping relationship between HVS$\bar{Q}_j$ and $\phi_j$ is simulated and analyzed in the case of $W_y = 30 \sim 3000$N, as shown in Fig. 5. It can be seen from Fig. 5 (a) and (b) that $\bar{Q}_{j,x}(\phi_j)$ and $\bar{Q}_{j,y}(\phi_j)$ increase with $W_y$ varying from 30N to 3000N, which matches with Eq. (1). In addition, the increase of the load also leads to the increase of the load interval. However, it can be seen from Fig. 5 (c) that the mapping relationship between HVS$\bar{Q}_j$ and $\phi_j$ is completely unaffected by the change of load. Actually, it can be known from Eq. (6) that HVS$\bar{Q}_j$ is only affected by $\phi_j$, and it is most remarkable that the relationship between HVS$\bar{Q}_j$ and $\phi_j$ is almost linear in the main load interval (240° ∼300°), as shown in Fig. 5 (c).

### B. THE MAPPING RELATIONSHIP BETWEEN $HVS\Delta\bar{Q}_f$ AND THE OUTER RACEWAY DEFECT ANGULAR POSITION

This section investigates the influence of the outer raceway defect angular position $\phi_f$ on the contact forces. The static contact forces between the ball $j$ and raceways in the $x$ and $y$ directions for a defective bearing with an outer raceway defect are named as $\bar{Q}^d_{j,x}$ and $\bar{Q}^d_{j,y}$ in order to distinguish them from the forces for failure-free bearings. The circumferential extent and depth were set to $\Delta\phi_f = 1°$ and $h = 0.1$mm, respectively. The load is still set as $W_x = 0$ and $W_y = -100$. Fig. 6 presents the variation curve of $\bar{Q}^d_{j,x}$ and $\bar{Q}^d_{j,y}$ in the case of $\phi_f = 250°$. As observed in Fig. 6, irrespective of the $x$ or $y$ direction, once the ball $j$ passes through the defect zone, the contact force of the ball $j$ will appear mutation. Furthermore, both $\bar{Q}^d_{j,x}(\phi_j)$ and $\bar{Q}^d_{j,y}(\phi_j)$ reach the extremum $\bar{Q}^d_{f,x}$ and $\bar{Q}^d_{f,y}$ when the ball $j$ is arriving at the defect center, namely, $\bar{Q}^d_{f,x} = \bar{Q}^d_{j,x}(\phi_j = \phi_f)$, $\bar{Q}^d_{f,y} = \bar{Q}^d_{j,y}(\phi_j = \phi_f)$. Applying Eqs. (1)-(6) gives

$$\begin{cases} \bar{Q}^d_{f,x} = K\left(\delta_f\right)_+^{1.5}\cos\phi_f \\ \bar{Q}^d_{f,y} = K\left(\delta_f\right)_+^{1.5}\sin\phi_f \\ HVS\bar{Q}_f = \left|\dfrac{\bar{Q}^d_{f,x}}{\bar{Q}^d_{f,y}}\right| = \left|\cot\phi_f\right| \end{cases} \tag{7}$$

where $\delta_f$ is the contact deformation of the ball $j$ located at the defect center, namely, $\delta_f = \delta_j(\phi_j = \phi_f)$. With Eq. (7), the variation curves of $\bar{Q}^d_{f,x}$ and $\bar{Q}^d_{f,y}$ with the change of $\phi_f$ in load interval [206.3°, 333.8°] can be solved, as shown in Fig.7 (a) and (b). Fig. 7 shows that $\bar{Q}^d_{f,x}$ and $\bar{Q}^d_{f,y}$ are equal to zero in the load interval [206.3°, 218.1°] and [332.0°, 333.8°]. That is to say, the ball located at $\phi_f$ is unloaded. It is caused by two factors: 1) the two intervals are close to the unloaded interval. Combined with Fig. 4, it can be concluded that even for a failure-free bearing system, the ball contact force is very small in the two intervals, that is, the contact deformation $\delta_f$ is very small. 2) when the defect is located in the two intervals, it can be obtained from Eq. (3) that $\delta_f$ becomes to be non-positive influenced by the effective defect depth $d$, resulting in $\bar{Q}^d_{f,x} = \bar{Q}^d_{f,y} = 0$.

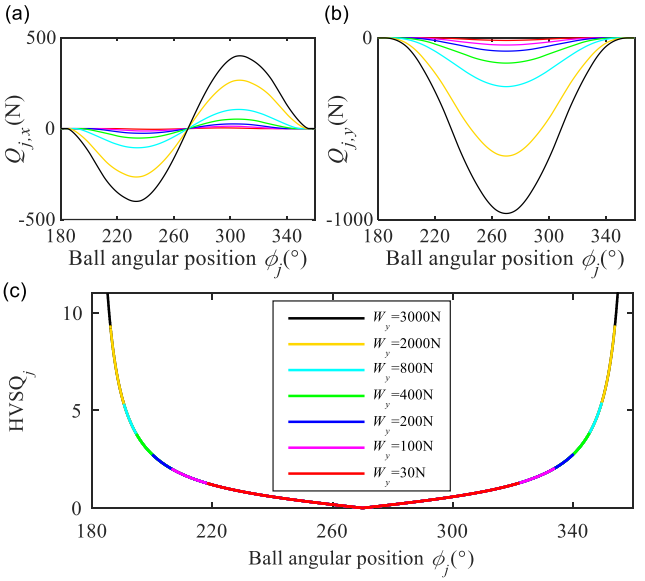


**FIGURE 5.** Static contact forces and HVS$\bar{Q}_j$ under different load conditions: (a)$\bar{Q}_{j,x}(\phi_j)$; (b)$\bar{Q}_{j,y}(\phi_j)$; (c) HVS$\bar{Q}_j(\phi_j)$.

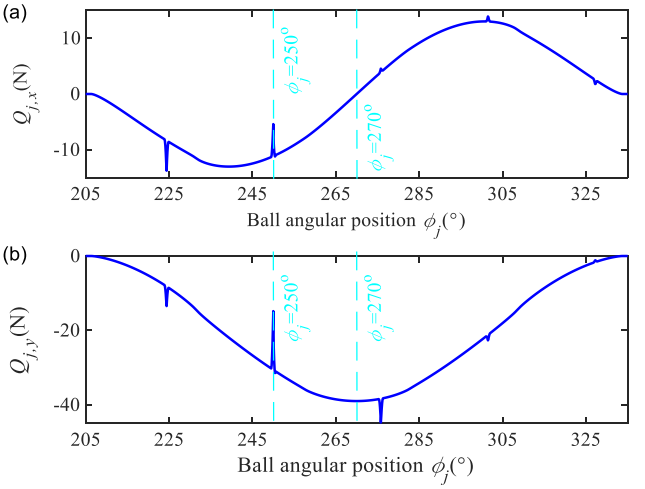


**FIGURE 6.** Static contact forces of the ball $j$ for a defective bearing with an outer raceway defect: (a)$\bar{Q}^d_{j,x}(\phi_j)$; (b)$\bar{Q}^d_{j,y}(\phi_j)$.

Most noteworthy, it can be known from Eq. (7) that $\bar{Q}^d_{f,x}$ and $\bar{Q}^d_{f,y}$ are affected by many factors, such as the load, the defect angular position and the ball number. However, HVS$\bar{Q}_f$ is a univariate function with the defect angular position $\phi_f$ as the variable. In addition, HVS$\bar{Q}_f$ distributes symmetrically by the angle position 270° for the center, and has the relation of approximate linear change with defect angle position $\phi_f$ in the main load interval (240° ∼300°), as shown in Fig. 7(c). $\Delta\bar{Q}_{f,x}$ and $\Delta\bar{Q}_{f,y}$ represent the value of the difference between the contact forces of ball $j$ for a failure-free bearing and a defective bearing of ball angular position $\phi_j = \phi_f$. Combined with Eq. (6) and (7), HVS$\Delta\bar{Q}_f$ can be expressed as follows

$$HVS\Delta\bar{Q}_f = \left|\frac{\Delta\bar{Q}_{f,x}}{\Delta\bar{Q}_{f,y}}\right| = \left|\frac{\bar{Q}_{j,x}(\phi_j=\phi_f) - \bar{Q}^d_{f,x}}{\bar{Q}_{j,y}(\phi_j=\phi_f) - \bar{Q}^d_{f,y}}\right| = \left|\cot\phi_f\right| \tag{8}$$

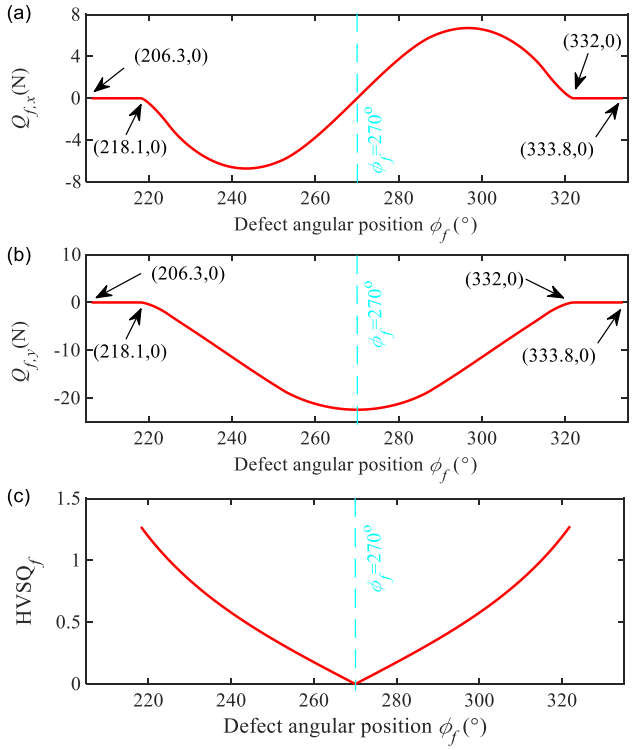


**FIGURE 7.** Variation curves of the extremum of contact force for the ball $j$ passing through the defect zone varying with $\phi_f$: (a) $\bar{Q}^d_{f,x}(\phi_f)$; (b) $\bar{Q}^d_{f,y}(\phi_f)$; (c) HVS$\bar{Q}_f(\phi_f)$.

From Eq. (8), it can be noted that HVS$\Delta\bar{Q}_f$ is a cotangent function with $\phi_f$ as the only variable. The value of the difference for the contact force caused by a ball passing the defect zone is the main excitation source of the vibration acceleration response of the bearing system, which reveals the advantage and the necessity of the horizontal-vertical synchronization signal analysis for defect localization of the outer raceway defect in essence.

## III. DYNAMIC MODEL AND THE HORIZONTAL-VERTICAL SYNCHRONIZATION SIGNAL ANALYSIS

In Section II, the relationships between the contact force and the defect angular position of the static model in the cases of failure-free and defective are studied. To reveal the mechanism of the corresponding relationships for the actual system more realistically, the horizontal-vertical synchronization signal analysis based on the dynamic model of a bearing system is carried out in this section. The dynamic equations of the ball bearing shown in Fig. 1 can be expressed as

$$\begin{cases} m_i\ddot{x}_i + c_{ix}\dot{x}_i + k_{ix}x_i = W_x - Q_x - Q_{dx} \\ m_i\ddot{y}_i + c_{iy}\dot{y}_i + k_{iy}y_i = W_y - Q_y - Q_{dy} \\ m_o\ddot{x}_o + c_{ox}\dot{x}_o + k_{ox}x_o = Q_x + Q_{dx} \\ m_o\ddot{y}_o + c_{oy}\dot{y}_o + k_{oy}y_o = Q_y + Q_{dy} \end{cases} \tag{9}$$

where $Q_x$ and $Q_y$ are the dynamic contact forces in the $x$ and $y$ directions, $Q_{dx}$ and $Q_{dy}$ are the dynamic contact damping forces in the $x$ and $y$ directions. Eq. (9) shows a typical multi-freedom nonlinear self-excited vibration system. It is difficult to obtain its analytical solution directly. This paper will analyze it from three aspects: high-precision numerical solution, simplified analysis solution and linearization analysis. Firstly, Eq. (9) was solved numerically by the ODE 45 solver in MATLAB. The main parameters of the bearing system can be found in Ref. [23]. Hence, the dynamic contact force and vibration acceleration of the outer raceway were obtained.

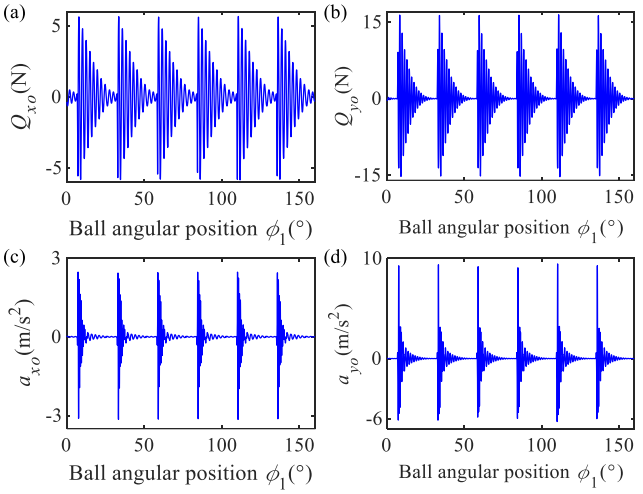


**FIGURE 8.** Dynamic contact forces and vibration acceleration of the outer raceway for a defective bearing with an outer raceway defect: (a)$Q_{xo}(\phi_1)$; (b)$Q_{yo}(\phi_1)$; (c)$a_{xo}(\phi_1)$; (d)$a_{yo}(\phi_1)$.

The dynamic contact force and vibration acceleration response of a ball bearing system with an outer raceway defect of the angular position $\phi_f = 270°$, circumferential extent $\Delta\phi_f = 1°$ and depth $h = 0.3$mm are numerically solved with the ODE function in Matlab by substituting Eqs. (1) - (4) into Eq. (9), as shown in Fig. 8. According to Fig. 8 (a) and (b), it can be seen that the peak of the resultant contact force increases significantly when the ball passes the outer raceway defect. This results in a significant increase of the peak of the vibration acceleration. Therefore, this indicates that the peak of vibration acceleration of the outer raceway defect bearing depends on the difference value of the contact force caused by a ball passing the defect. To obtain the approximate analytical relationship between the defect angular position and the vibration acceleration, the multi-degree freedom dynamic model of the bearing system represented in Fig. 1 and Eq. (9) is simplified as a single-degree-freedom system. Taking the vibration in the $x$ direction of the outer ring as an example, the contact damping term is ignored, and for the failure-free system, the dynamic contact force can be approximately replaced by the static contact force. Therefore, the dynamic equation is defined as

$$m_o\ddot{x}_o + c_o\dot{x}_o + k_o x_o = \bar{Q}_x \tag{10}$$

According to Section I, it can be seen that the external excitation force $\bar{Q}_x$ of the single-degree-freedom system is the linear superposition of the contact forces $\bar{Q}_{j,x}$. It can be

seen from Eq. (5) that for the failure-free case, $\bar{Q}_{j,x}$ is approximately a sine function. Therefore, the vibration response of the single-degree-freedom system under the excitation $\bar{Q}_{j,x}$ can be expressed as

$$\bar{x}_{j,o}(t)=\frac{A_x}{\sqrt{\left(k_o-m_o\omega_q^2\right)^2+c_o^2\omega_q^2}}\cos\left(\omega_q t-\phi_q\right) \tag{11}$$

where

$$\phi_q=\arctan\left(\frac{c_o\omega_q}{k_o-m_o\omega_q^2}\right) \tag{12}$$

Similarly, for the single-degree-freedom system of the outer race in the $y$ direction, the vibration response under the excitation of $\bar{Q}_{j,y}$ can be calculated here as follows

$$\bar{y}_{j,o}(t)=\frac{A_y}{\sqrt{\left(k_o-m_o\omega_q^2\right)^2+c_o^2\omega_q^2}}\cos\left(\omega_q t-\phi_q\right)-\frac{A_y}{k_o} \tag{13}$$

Eq. (11) and Eq. (13) represent the vibration responses of a failure-free system. When a defect of $\Delta\phi_f = 1^\circ$ and $h = 0.3$mm occurs in the outer raceway, the contact force of the ball $j$ passing through the defect is defined by

$$Q_{j,x}^d=\bar{Q}_{j,x}+\Delta\bar{Q}_{j,x},\ Q_{j,y}^d=\bar{Q}_{j,y}+\Delta\bar{Q}_{j,y} \tag{14}$$

where $\Delta\bar{Q}_{j,x}$ and $\Delta\bar{Q}_{j,y}$ represent the value of the difference between the contact forces of the ball $j$ for a failure-free bearing and a defective bearing when the ball $j$ locates at the defect zone. The effects of $\Delta\bar{Q}_{j,x}$ and $\Delta\bar{Q}_{j,y}$ on the single-degree-freedom systems can be expressed as impulse excitations, that is

$$\begin{cases}\underset{\sim}{Q}_x=\int_t^{t+\Delta t}\Delta\bar{Q}_{j,x}dt=\Delta\bar{Q}_{f,x}\Delta t\\ \underset{\sim}{Q}_y=\int_t^{t+\Delta t}\Delta\bar{Q}_{j,y}dt=\Delta\bar{Q}_{f,y}\Delta t\end{cases} \tag{15}$$

where $\Delta t$ is the duration of the ball passing through the defect zone. The response of the single-degree-freedom system of the outer race in the $x$ and $y$ directions under the excitation of $\Delta\bar{Q}_{f,x}$ and $\Delta\bar{Q}_{f,y}$ can be expressed as

$$\underset{\sim}{x}_o(t)=\frac{\underset{\sim}{Q}_x\,e^{-\xi\omega_n t}}{m_o\omega_d}\sin\omega_d t,\quad \underset{\sim}{y}_o(t)=\frac{\underset{\sim}{Q}_y\,e^{-\xi\omega_n t}}{m_o\omega_d}\sin\omega_d t \tag{16}$$

where

$$\omega_n=\sqrt{k_o/m_o},\quad \xi=c_o/2m\omega_n,\ \omega_d=\omega_n\sqrt{1-\xi^2} \tag{17}$$

The total responses of the outer race with a defect in the $x$ and $y$ directions are defined as

$$x_o(t)=\sum_{j=1}^{N_b}\bar{x}_{j,o}(t)+\underset{\sim}{x}_o(t),\quad y_o(t)=\sum_{j=1}^{N_b}\bar{y}_{j,o}(t)+\underset{\sim}{y}_o(t) \tag{18}$$

Substituting Eqs. (11)-(17) into Eq. (18) and gaining the quadric derivative, the vibration acceleration responses can be expressed as

$$\begin{aligned}a_{x,o}(t)&=\sum_{j=1}^{N_b}\bar{a}_{j,x}(t)+\underset{\sim}{a}_{x,o}(t),\\ a_{y,o}(t)&=\sum_{j=1}^{N_b}\bar{a}_{j,y}(t)+\underset{\sim}{a}_{y,o}(t)\end{aligned} \tag{19}$$

where

$$\begin{cases}\bar{a}_{j,x}(t)=\dfrac{-A_x\omega_q^2}{\sqrt{\left(k_o-m_o\omega_q^2\right)^2+c_o^2\omega_q^2}}\cos\left(\omega_q t-\phi_q\right)\\ \underset{\sim}{a}_{x,o}(t)=\dfrac{\omega_n\underset{\sim}{Q}_x}{m_o\sqrt{1-\xi^2}}e^{-\xi\omega_n t}\\ \sin\left(\omega_d t+\arctan\dfrac{2\xi^2-1}{2\xi\sqrt{1-\xi^2}}\right)\\ \bar{a}_{j,y}(t)=\dfrac{-A_y\omega_q^2}{\sqrt{\left(k_o-m_o\omega_q^2\right)^2+c_o^2\omega_q^2}}\cos\left(\omega_q t-\phi_q\right)\\ \underset{\sim}{a}_{y,o}(t)=\dfrac{\omega_n\underset{\sim}{Q}_y}{m_o\sqrt{1-\xi^2}}e^{-\xi\omega_n t}\\ \sin\left(\omega_d t+\arctan\dfrac{2\xi^2-1}{2\xi\sqrt{1-\xi^2}}\right)\end{cases} \tag{20}$$

According to ISO standard, this paper makes a general comparison and analysis of the peak value of $\bar{a}_{j,x}(t)$ and $\underset{\sim}{a}_{x,o}(t)$ in the rated load range of the selected NSK6308 ball bearing, that is

$$\frac{A_x\omega_q^2m_o\sqrt{1-\xi^2}}{\omega_n\Delta Q_x\Delta t\sqrt{\left(k_o-m_o\omega_q^2\right)^2+c_o^2\omega_q^2}}<\frac{A_x\omega_q^2m_o^{1.5}}{\Delta Q_x\Delta t k_o^{1.5}}<10^{-3} \tag{21}$$

Eq. (21) illustrates that the peak of $\bar{a}_{j,x}(t)$ is far less than the peak of $\underset{\sim}{a}_{x,o}(t)$. Similarly, the conclusion is also appropriate for the peak of $\bar{a}_{j,y}(t)$ and $\underset{\sim}{a}_{y,o}(t)$. Therefore, the peaks $P_{x,o}$ and $P_{y,o}$ of $a_{x,o}(t)$ and $a_{y,o}(t)$ are expressed as

$$\begin{aligned}P_{x,o}&=\omega_n\underset{\sim}{Q}_x\Big/m_o\sqrt{1-\xi^2},\\ P_{y,o}&=\omega_n\underset{\sim}{Q}_y\Big/m_o\sqrt{1-\xi^2}\end{aligned} \tag{22}$$

According to the above analysis, the horizontal-vertical synchronization peak (HVSPeak) proposed in this paper is defined as

$$\text{HVSPeak}=\left|P_{x,o}/P_{y,o}\right| \tag{23}$$

Then, combining Eqs. (8), (15), (22) and (23), the theoretical relationship between HVSPeak and $\phi_f$ can be obtained as:

$$\text{HVSPeak}(\phi_f)=\left|\cot\left(\phi_f\right)\right| \tag{24}$$

Eq. (24) shows that HVSPeak is approximately a cotangent function that takes $\phi_f$ as the only variable and factor. In section II, it has been proved based on Eq. (7) and Fig. 6(c) that for the static system, when the ball passes through the defect zone, although the value of $\bar{Q}^d_{j,x}$ and $\bar{Q}^d_{j,y}$ are affected by multiple factors, HVS$\bar{Q}_f$ and HVS$\Delta\bar{Q}_f$ are both the cotangent functions with $\phi_f$ as the only variable. To verify the applicability of this property in the nonlinear dynamic system, the relationship between HVSQ$_f$ of the dynamic system and $\phi_f$ is simulated by the numerical solution of Eq. (9), as the red line shown in Fig. 9. It can be seen that the relationship of HVSQ$_f$ and $\phi_f$ is also approximately a cotangent function.

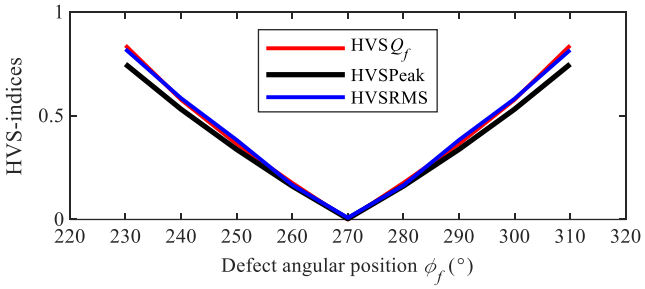


**FIGURE 9.** Variation curves of HVS$Q_f$ (red), HVSPeak (black) and HVSRMS (blue) varying with $\phi_f$ for simulated vibration responses.

With Eq. (23) and the numerical solution of Eq. (9), the variation curve of HVSPeak with the change of the defect angular position $\phi_f$ was simulated, as the black line shown in Fig. 9. It can be seen that the relationship between HVSPeak and $\phi_f$ is approximately a cotangent function, which verifies the accuracy of Eq. (24).

However, the stability of the peak is highly susceptible to the noise and other factors in actual signals. To overcome this problem, and on account of the linear relationship between the peak and RMS for the exponential attenuation function, the horizontal-vertical synchronization RMS (HVSRMS) is proposed as

$$HVSRMS = \mathrm{RMS}_{ax} / \mathrm{RMS}_{ay} \tag{25}$$

and the theoretical relationship between HVSRMS and $\phi_f$ is shown as:

$$\mathrm{HVSRMS}(\phi_f) = \left|\cot\left(\phi_f\right)\right| \tag{26}$$

where $\mathrm{RMS}_{ax}$ and $\mathrm{RMS}_{ay}$ are the root-mean-square values of the horizontal and vertical vibration acceleration signal for the bearing system, respectively. With Eq. (25) and the numerical solution of Eq. (9), the curve of HVSRMS changing with $\phi_f$ is calculated as the blue line shown in Fig. 9, which indicates that HVSRMS is approximately a cotangent function that takes $\phi_f$ as the variable, which verifies the accuracy of Eq. (26). By now, the mathematical and physical nature of the approximate linear relationship between HVSRMS and $\phi_f$ on both sides of 270°, proposed by reference [1] through qualitative analysis and numerical simulation, is revealed, and a more accurate functional relationship between them is obtained. Predictably, HVSRMS is a practical diagnostic feature for the angular position estimation of the outer raceway defect.

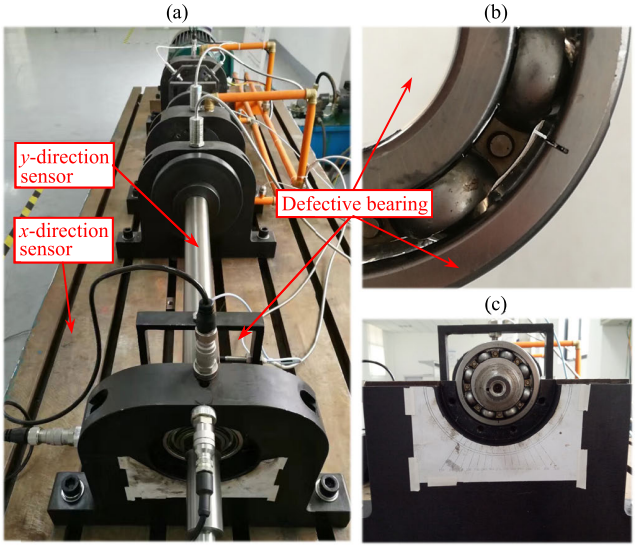


**FIGURE 10.** Photos of experimental apparatus: (a) The bearing test rig; (b) Defective bearing with defect size of $\Delta\phi_f = 1°$; (c) The bearing pedestal.

## IV. EXPERIMENTAL VERIFICATION AND METHOD COMPARISON

The experimental apparatus, applied to acquire actual signals of a ball bearing with an outer raceway defect and verify the effectiveness of the method proposed in this paper, is shown in Fig. 10. The bearing is NSK6308, and has $N_b = 8$ balls. The shaft frequency and sample frequency were set to $f_s = 7$Hz and $F_s = 65536$, respectively. The sampling points is $N = 131073$. The wire cutting method is used to process an outer raceway defect of circumferential extent $\Delta\phi_f = 1°$, depth $h = 0.3$mm. The vertical ($y$) and horizontal ($x$) direction vibration acceleration signal for the defect angular position $\phi_f = 240° \sim 300°$ are measured at intervals of 10°. Fig. 11 shows the time-domain waveform of the measured vibration acceleration signal for $\phi_f = 240°$. It can be seen that due to the existence of the outer raceway defect, the acceleration signals in the $x$ and $y$ directions both vibrate at the same period. Moreover, the peak of the vibration in the $x$ direction is significantly lower than that of the $y$ direction. These characteristics are consistent with the simulation results shown in Fig. 8. To verify the applicability of HVSPeak and HVSRMS in actual signals, the results of the measured signals were solved.

With the definitions in section III, HVSRMS and HVSPeak at different defect angular positions are solved and normalized for observation, as shown in Fig. 12. It can be seen from Fig. 12 that the curve of HVSPeak for the measured vibration signal varying with $\phi_f$ is not only non-linear, but also non-monotonic. It confirms the prediction in section III: although the relationship between HVSPeak and $\phi_f$ is an approximate linear relationship in theoretically, actual signals

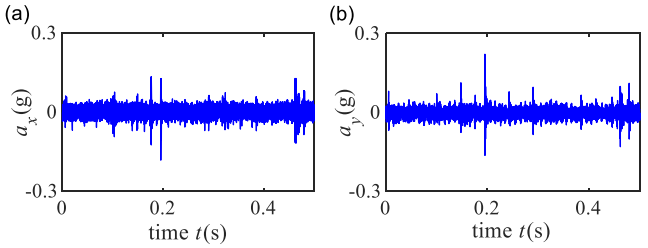


**FIGURE 11.** Measured vibration acceleration signal for the case of $\Delta\phi_f = 1°$ and $\phi_f = 240°$: (a) Horizontal acceleration $a_x(t)$; (b) Vertical acceleration $a_y(t)$.

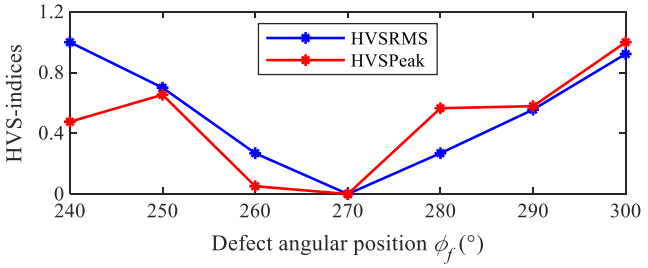


**FIGURE 12.** Variation curves of HVS-indices varying with $\phi_f$ for the measured vibration acceleration signal: HVSPeak (red), HVSRMS (blue).

are susceptible to noise and other factors, which affects the applicability and accuracy of HVSPeak.

Comparing with Fig. 9 and Fig. 12, it can be seen that the HVSRMS of the measured signal gradually exhibits the symmetrical distribution centered on $\phi_f = 270°$, and has the relation of approximate linear change with $\phi_f$, which verifies the simulation results and Eq. (26) in section III.

To further verify the necessity and superiority of HVSRMS, Fig. 13 shows curves of some common indices varying with $\phi_f = 240° \sim 300°$ for the measured horizontal and vertical acceleration signals, including RMS, Kurtosis, CF, Sr, S$\alpha$ [1], SampEn [25] and LempelZiv [26]. Since the magnitudes of the different indicators are different, all indicators are normalized in Figure 13 for ease of observation. It can be seen from Fig. 13 (a) and (b) that all of these indices do not have any monotonicity variation relationship with $\phi_f$, so they have no ability to locate the angular position of the outer raceway defect. This adequately approves the effectiveness and superiority of the HVSRMS method for localization diagnosis of outer raceway defect in ball bearings.

It should be noticed that the noise in the measured signals may interfere the calculation results of HVSRMS, thus affecting the diagnostic accuracy. For example, there is an obvious deviation of the HVSRMS curve on the left side of 270° in Fig. 12, especially at $\phi_f = 250°$. To this end, three methods of lifting wavelet, morphological filtering and matching pursuit are applied to the measured signal preprocess, where the signal processing method suitable for HVSRMS is highlighted to improve the localization accuracy. Due to the space limit, only the original signal and the processed signals by the three methods in the case of $\phi_f = 260°$ are given here,

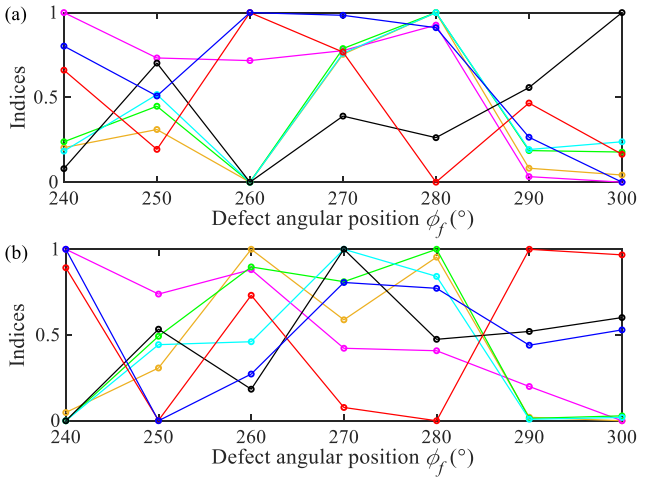


**FIGURE 13.** Variation curves of RMS(—), Kurtosis(—), CF(—), Sr(—), S$\alpha$(—), SampEn(—) and LempelZiv(—) varying with $\phi_f = 240° \sim 300°$ for the measured (a) Horizontal acceleration signals and (b) Vertical acceleration signals.

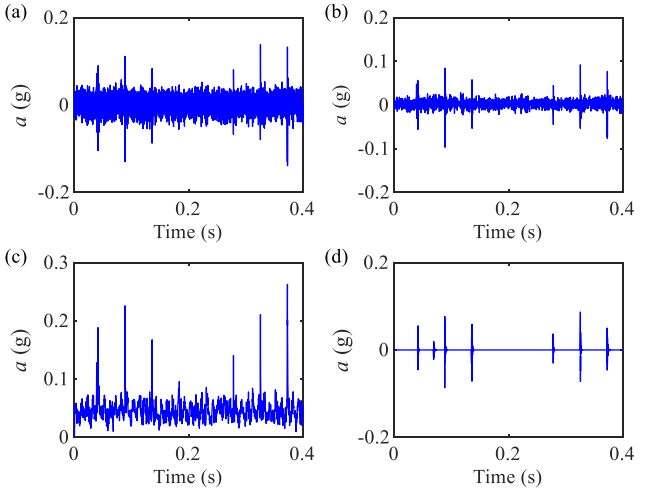


**FIGURE 14.** The processing results of measured horizontal vibration signals for the case of $\phi_f = 260°$ using the three methods: (a) Original signal; (b) Lifting wavelet; (c) Morphological filtering; (d) Matching pursuit.

as shown in Fig. 14. It can be seen from Fig. 14 that the signal-to-noise ratio of the signals processed by the three methods is significantly improved, and the mature spectrum analysis methods such as Hilbert envelope spectrum is sufficient to qualitatively diagnose the bearing outer ring fault.

However, it does not mean that all three methods can effectively improve the accuracy of the HVSRMS index of the measured signal. Fig. 15 shows the curves of HVSRMS varying with $\phi_f$ of the measured signals processed by the three methods. It can be found that the morphological filtering method can significantly improve the accuracy of HVSRMS, followed by the lifting wavelet method, while the result of the matching pursuit method is totally ineffective. It can be explained combined with the definition of HVSRMS and its mathematical nature in the previous section that although the matching pursuit method can greatly improve the

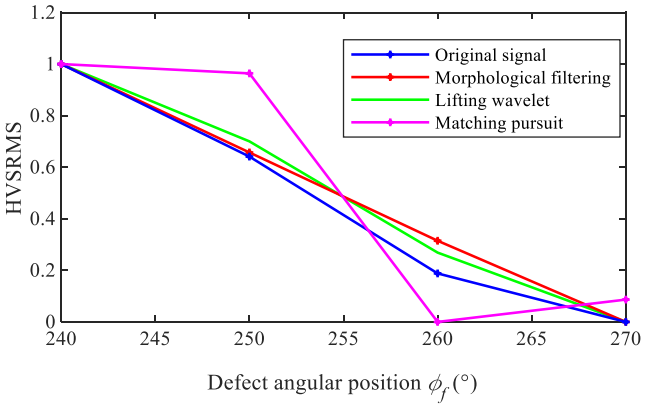


**FIGURE 15.** Variation curves of HVSRMS varying with $\phi_f$ for the measured vibration acceleration signals processed by the three methods.

signal-to-noise ratio, it cannot accurately maintain the amplitude information of the fault impulse waveform, as shown in Fig. 14(d). This is a common problem in existing sparse decomposition methods. It can be seen from Fig. 14(b) that the lifting wavelet method maintains the amplitude of the fault impact waveform while reducing noise, thus improving the accuracy of HVSRMS. As can be seen from Fig. 14(c), the morphological filtering method significantly increases the amplitude of the fault impulse waveform while suppressing noise. Besides, the most critically, the fault impulse waveform in the $x$- and $y$-direction is scaled up meanwhile, which makes the morphological filtering method achieve the best results. This discovery can be used to indicate the direction of the subsequent signal processing methods for HVSRMS: 1. Research a noise reduction method that does not cause amplitude distortion of the fault impulse waveform. 2. Develop a method that can proportionally enhance the fault impulse waveform of the $x$-direction and $y$-direction signals. 3. Improve the existing sparse decomposition and other methods with the goal that reserve the amplitude information of the fault impulse waveform accurately.

## V. CONCLUSION

In-depth discussion and demonstration about the localization of the outer raceway defect on the ball bearing were carried out in this paper. Firstly, based on the mathematical derivation and solution of the static model, it shows that the extremums of the contact component forces $\bar{Q}^d_{f,x}$ and $\bar{Q}^d_{f,y}$ of the ball passing through the defect zone are respectively the sine and versine functions that take the defect angular position $\phi_f$, the external load and bearing parameters as variables. However, HVS$\bar{Q}_f$ and HVS$\Delta\bar{Q}_f$ are both cotangent functions that take $\phi_f$ as the only variable. These findings reveal the mechanism and basis of the HVS-index method to realize the localization diagnosis of outer raceway defect in essence.

On that basis, the numerical simulation and approximate analytical analysis of the nonlinear dynamic model of the bearing system are carried out. It is confirmed that both HVS$Q_f$ and HVS$\Delta Q_f$ in the dynamic system are approximately cotangent functions that take $\phi_f$ as the only variable. Then two localization diagnosis indices: horizontal–vertical synchronized Peak (HVSPeak) and horizontal–vertical synchronized RMS (HVSRMS) were proposed. Theoretical analysis and simulation results show that HVSPeak and HVSRMS are also approximately cotangent functions that take $\phi_f$ as the only variable, that is to say, both curves of HVSPeak and HVSRMS varying with $\phi_f$ are approximately two fixed gradient lines with symmetrical about $\phi_f = 270°$ in the interval of [240°, 300°]. In addition, the function is not affected by any other factors except $\phi_f$ in theory. This feature is similar to the defect characteristic frequency that the qualitative diagnosis relies on, which provides support for the localization of outer raceway defect. Then, based on the analysis of the measured signal acquired from the experimental apparatus, the applicability and accuracy of HVSRMS in localization of outer raceway defect are verified. More importantly, the necessity and superiority of HVSRMS is highlighted by comparing with HVSPeak, RMS, Kurtosis, CF, $S_r$, $S_\alpha$, SampEn and LempelZiv.

Finally, the effects of three signal processing methods, lifting wavelet, morphological filtering and matching pursuit, are compared to solve the problem that noises in actual signals interfere the accuracy of localization diagnosis based on HVSRMS. The results show that the morphological filtering method has the best extraction effect, and the matching pursuit method has the worst effect, even counterproductive. Combining with the mathematical mechanism of HVSRMS and the characteristics of the three methods, the principle is explained, and the following directions are pointed out for the research of signal processing methods on HVSRMS: 1. Research a noise reduction method that does not cause amplitude distortion of the impact waveform. 2. Develop a method that can proportionally enhance the fault impulse waveform of the $x$-direction and $y$-direction signals. 3. Improve the existing sparse decomposition and other methods with the goal that reserve the amplitude information of the fault impulse waveform accurately.

## REFERENCES

[1] L. Cui, J. Huang, and F. Zhang, "Quantitative and localization diagnosis of a defective ball bearing based on vertical–horizontal synchronization signal analysis," *IEEE Trans. Ind. Electron.*, vol. 64, no. 11, pp. 8695–8705, Nov. 2017.

[2] T. Wang, Q. Han, F. Chu, and Z. Feng, "Vibration based condition monitoring and fault diagnosis of wind turbine planetary gearbox: A review," *Mech. Syst. Signal Process.*, vol. 126, pp. 662–685, Jul. 2019.

[3] T. Wang, M. Liang, J. Li, and W. Cheng, "Rolling element bearing fault diagnosis via fault characteristic order (FCO) analysis," *Mech. Syst. Signal Process.*, vol. 45, pp. 139–153, Mar. 2014.

[4] W. Li, S. Zhang, and S. Rakheja, "Feature denoising and nearest–farthest distance preserving projection for machine fault diagnosis," *IEEE Trans. Ind. Informat.*, vol. 12, no. 1, pp. 393–404, Feb. 2016.

[5] B. Yang, R. Liu, and X. Chen, "Fault diagnosis for a wind turbine generator bearing via sparse representation and shift-invariant K-SVD," *IEEE Trans. Ind. Informat.*, vol. 13, no. 3, pp. 1321–1331, Jun. 2017.

[6] N. Li, Y. Lei, J. Lin, and S. X. Ding, "An improved exponential model for predicting remaining useful life of rolling element bearings," *IEEE Trans. Ind. Electron.*, vol. 62, no. 12, pp. 7762–7773, Dec. 2015.

[7] Y. Lei, F. Jia, J. Lin, S. Xing, and S. X. Ding, "An intelligent fault diagnosis method using unsupervised feature learning towards mechanical big data," *IEEE Trans. Ind. Electron.*, vol. 63, no. 5, pp. 3137–3147, May 2016.

[8] R. K. Singleton, E. G. Strangas, and S. Aviyente, "The use of bearing currents and vibrations in lifetime estimation of bearings," *IEEE Trans. Ind. Informat.*, vol. 13, no. 3, pp. 1301–1309, Jun. 2017.
[9] S. R. Saufi, Z. A. B. Ahmad, M. S. Leong, and M. H. Lim, "Low-speed bearing fault diagnosis based on ArSSAE model using acoustic emission and vibration signals," *IEEE Access*, vol. 7, pp. 46885–46897, 2019.
[10] Z. Li, A. Ming, W. Zhang, T. Liu, F. Chu, and Y. Li, "Fault feature extraction and enhancement of rolling element bearings based on maximum correlated kurtosis deconvolution and improved empirical wavelet transform," *Appl. Sci.*, vol. 9, no. 9, p. 1876, 2019.
[11] M. Van and H.-J. Kang, "Bearing defect classification based on individual wavelet local Fisher discriminant analysis with particle swarm optimization," *IEEE Trans. Ind. Informat.*, vol. 12, no. 1, pp. 124–135, Feb. 2016.
[12] Y. Kong, T. Wang, and F. Chu, "Meshing frequency modulation assisted empirical wavelet transform for fault diagnosis of wind turbine planetary ring gear," *Renew. Energy*, vol. 132, pp. 1373–1388, Mar. 2019.
[13] Y. Li, M. Xu, X. Liang, and W. Huang, "Application of bandwidth EMD and adaptive multiscale morphology analysis for incipient fault diagnosis of rolling bearings," *IEEE Trans. Ind. Electron.*, vol. 64, no. 8, pp. 6506–6517, Aug. 2017.
[14] L. Cui, N. Wu, C. Ma, and H. Wang, "Quantitative fault analysis of roller bearings based on a novel matching pursuit method with a new step-impulse dictionary," *Mech. Syst. Signal Process.*, vols. 68–69, pp. 34–43, Feb. 2016.
[15] M. Singh, R. K. Yadav, and R. Kumar, "Discrete wavelet transform based measurement of inner race defect width in taper roller bearing," *MAPAN*, vol. 28, no. 1, pp. 17–23, Mar. 2013.
[16] S. Zhao, L. Liang, G. Xu, J. Wang, and W. Zhang, "Quantitative diagnosis of a spall-like fault of a rolling element bearing by empirical mode decomposition and the approximate entropy method," *Mech. Syst. Signal Process.*, vol. 40, no. 1, pp. 154–177, Oct. 2013.
[17] M. Zhao, J. Lin, Y. Miao, and X. Xu, "Detection and recovery of fault impulses via improved harmonic product spectrum and its application in defect size estimation of train bearings," *Measurement*, vol. 91, pp. 421–439, Sep. 2016.
[18] A.-B. Ming, W. Zhang, Z.-Y. Qin, and F.-L. Chu, "Dual-impulse response model for the acoustic emission produced by a spall and the size evaluation in rolling element bearings," *IEEE Trans. Ind. Electron.*, vol. 62, no. 10, pp. 6606–6615, Oct. 2015.
[19] L. Niu, H. Cao, Z. He, and Y. Li, "Dynamic modeling and vibration response simulation for high speed rolling ball bearings with localized surface defects in raceways," *J. Manuf. Sci. Eng.*, vol. 136, no. 4, May 2014, Art. no. 041015.
[20] S. Khanam, J. K. Dutt, and N. Tandon, "Impact force based model for bearing local fault identification," *J. Vib. Acoust.*, vol. 137, no. 5, Oct. 2015, Art. no. 051002.
[21] L. L. Cui, Y. Zhang, F. B. Zhang, J. Y. Zhang, and S. Lee, "Vibration response mechanism of faulty outer race rolling element bearings for quantitative analysis," *J. Sound Vibrat.*, vol. 364, pp. 67–76, Mar. 2016.
[22] J. Liu, Y. Shao, and W. D. Zhu, "A new model for the relationship between vibration characteristics caused by the time-varying contact stiffness of a deep groove ball bearing and defect sizes," *J. Tribol.*, vol. 137, no. 3, Jul. 2015, Art. no. 031101.
[23] D. Petersen, C. Howard, and Z. Prime, "Varying stiffness and load distributions in defective ball bearings: Analytical formulation and application to defect size estimation," *J. Sound Vib.*, vol. 337, pp. 284–300, Feb. 2015.
[24] L. Cui, J. Huang, F. Zhang, and F. Chu, "HVSRMS localization formula and localization law: Localization diagnosis of a ball bearing outer ring fault," *Mech. Syst. Signal Process.*, vol. 120, pp. 608–629, Apr. 2019.
[25] K. Zhu, X. Song, and D. Xue, "A roller bearing fault diagnosis method based on hierarchical entropy and support vector machine with particle swarm optimization algorithm," *Measurement*, vol. 47, pp. 669–675, Jan. 2014.
[26] L. Cui, X. Gong, J. Zhang, and H. Wang, "Double-dictionary matching pursuit for fault extent evaluation of rolling bearing based on the Lempel-Ziv complexity," *J. Sound Vib.*, vol. 385, pp. 372–388, Dec. 2016.

**FEIBIN ZHANG** received the B.S. degree from Jiangxi Agricultural University, Nanchang, China, in 2008, and the Ph.D. degree from the Beijing University of Technology, Beijing, China, in 2015, all in mechanical engineering. From 2014 to 2018, he was with the School of Mechanical Engineering, Jiangxi Agricultural University. He is currently a Postdoctoral Research Associate with the Department of Mechanical Engineering, Tsinghua University. His research interests include fault diagnosis and rotating machinery dynamics.

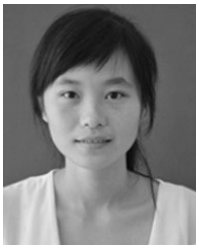

**JINFENG HUANG** received the B.S. degree in mechanical engineering from Jiangxi Agricultural University, Nanchang, China, in 2015, and the M.S. degree in mechanical engineering from the Beijing University of Technology, Beijing, China, in 2018. She is currently pursuing the Ph.D. degree in mechanical engineering with the Beijing University of Technology. Her research interests include fault detection and rotating machinery dynamic.

**FULEI CHU** received the B.S. degree in mechanical engineering from the Jiangxi University of Science and Technology, Ganzhou, China, in 1982, the M.S. degree in applied mechanics from Tianjin University, Tianjin, China, in 1985, and the Ph.D. degree in mechanical engineering from the University of Southampton, Southampton, U.K., in 1994. He is currently a Professor of vibration engineering with the Department of Mechanical Engineering, Tsinghua University, Beijing, China. His research interests include rotating machinery dynamics, machine condition monitoring and fault detection, nonlinear vibration, and vibration control.

**LINGLI CUI** received the B.S. degree in mechanical engineering from Shenyang Aerospace University, Shenyang, China, in 1998, the M.S. degree in mechanical engineering and automation from the Harbin Institute of Technology, Harbin, China, in 2001, and the Ph.D. degree in control theory and control engineering from the Institute of Automation, Chinese Academy of Sciences, Beijing, China, in 2004. She is currently a Professor of mechanical engineering with the Beijing University of Technology, Beijing. Her research interests include fault mechanisms, pattern recognition, intelligent diagnosis, and fault diagnosis.